THE ASTROPHYSICAL JOURNAL, 388:310–327, 1992 April 1

THE INTEGRATED SPECTRA OF NEARBY GALAXIES: GENERAL PROPERTIES AND EMISSION-LINE SPECTRA

ROBERT C. KENNICUTT, JR.[1]
Steward Observatory, University of Arizona, Tucson, AZ 85721
Received 1991 July 29; accepted 1991 September 11

ABSTRACT

This paper presents the first results from a survey of the integrated spectra of 90 nearby galaxies. Intermediate- and low-resolution spectrophotometry over the 3650–7000 Å range has been used to compile a spectral atlas of galaxies (published in a companion paper) and to investigate the systematic behavior of the emission-line spectra in normal and peculiar galaxies. The data are especially useful as a comparison sample for spectroscopic surveys of more distant galaxies.

The integrated absorption- and emission-line spectra show a smooth progression with Hubble type. Most spiral and irregular galaxies exhibit detectable emission lines of Hα, [O II], [N II], [S II], and sometimes Hβ and [O III]. The Hα line is the strongest emission line and is most reliable quantitative tracer of the massive star formation rate, but the [O II] line provides a good substitute in high-redshift galaxies, where Hα is inaccessible. The Hβ and [O III] lines are unsatisfactory as star formation tracers in all but the strongest emission-line galaxies, due to variations in stellar absorption and excitation, respectively. Methods for distinguishing between distant starburst galaxies and active nuclei are discussed.

The new data are used to examine the statistical properties of the [O II] emission in galaxies, and to calibrate a mean relation between [O II] luminosity and the total star formation rate. Star formation rates derived from the [O II] line are less accurate than those derived from Hα, and comparable in accuracy to rates derived from the continuum fluxes and colors. However, the [O II] data are very useful for comparing the star formation properties of large samples of galaxies. The distribution of [O II] equivalent widths in our sample is in good agreement with previous surveys of nearby galaxies and very different from that observed for blue-selected galaxies at intermediate redshift. The [O II] distribution for faint galaxies is very similar to that which is observed for nearby Markarian galaxies.

Subject headings: galaxies: ISM — galaxies: photometry — galaxies: stellar content

1. INTRODUCTION

The integrated spectra of galaxies are powerful diagnostics of their stellar content, star formation rates, and evolutionary properties. For high-redshift galaxies, which are too distant to spatially resolve from the ground, integrated spectra provide virtually the only information on their stellar populations. Surveys of faint galaxies by several groups (e.g., Dressler & Gunn 1983; Couch & Sharples 1987; Broadhurst, Ellis, & Shanks 1988; Lavery & Henry 1988; Colless et al. 1990) have produced an extensive data base on the spectroscopic properties of galaxies at moderate redshifts ($z \sim 0.2$–0.7), and a few observations have been made to $z \sim 2$ (e.g., Elston et al. 1991).

Given the broad interest in the spectral properties of distant objects, surprisingly little is known about the integrated spectra of very nearby galaxies. Spectra covering the nuclear regions are available for large samples, but such data cannot be directly compared to the observations of distant galaxies, where the projected aperture diameter is typically several kiloparsecs or more. Large-aperture spectrophotometry has been obtained for a few objects by Wells (1972), Dressler & Gunn (1982), Bothun & Dressler (1986), and Silva (1991), while intermediate sample data, with typical projected apertures of a few kiloparsecs, are available for larger samples (Peterson et al. 1986; Gallagher, Bushouse, & Hunter 1989). The utility of these data is limited by a number of factors, however, including spatial undersampling (usually a small fraction of the disk), limited spectral coverage (typically ~3700–5000 Å in the rest frame), and an incomplete range of galaxy types and luminosities.

In order to provide a more comprehensive data set on the spectral properties of galaxies at visible wavelengths, new integrated spectrophotometry has been obtained for 90 nearby ($z \leq 0.03$) galaxies, covering a broad range in morphological types, luminosities, star formation properties, and nuclear types. The spectra cover the full visible spectrum (3700–6800 Å), with a range in spectral resolution (5–25 Å) and signal-to-noise ratio which matches or exceeds the available observations of more distant galaxies.

This survey was motivated by two primary scientific goals. One objective was to evaluate the reliability of the strong emission lines in the blue (Hβ, [O III] λ5007, [O II] λ3727) as quantitative tracers of the total massive star formation rate in galaxies. For nearby objects the Hα emission-line flux is an excellent star formation diagnostic (e.g., Kennicutt 1983), but Hα redshifts out of the visible window beyond $z \sim 0.4$. Several workers have used the Hβ or [O II] lines to study the evolutionary properties of more distant galaxies (e.g., Dressler et al. 1985; Couch & Sharples 1987; Broadhurst et al. 1988; Colless et al. 1990; Elston et al. 1991), but the accuracy of these lines for quantitative applications has never been fully tested. This survey provides a means of comparing the blue lines directly

[1] Visiting Astronomer, Kitt Peak National Observatory, National Optical Astronomical Observatories, which are operated by the Association of Universities for Research in Astronomy, Inc. (AURA), under cooperative agreement with the National Science Foundation.

against Hα and for calibrating the mean relations between line fluxes and the star formation rate.

A second objective of the survey was to compile a reference library of spectra for galaxies of different types, which can be used for a variety of other applications, such as the classification of unresolved galaxies observed at large distances, the spectroscopic identification of extended sources detected in infrared, radio, and X-ray surveys, and rudimentary spectral synthesis applications. A spectrophotometric atlas of galaxies selected from this survey will be published in a companion paper (Kennicutt 1992, hereafter Paper II). This paper contains a general description of the survey, and a detailed analysis of the integrated emission line spectra. Further papers in the series will deal with the absorption line spectra in normal and peculiar galaxies.

The remainder of this paper is organized as follows: § 2 describes the observational techniques, reduction methods, and observational errors. Section 3 provides a synopsis of the spectral properties of galaxies along the Hubble sequence and presents examples for both normal and peculiar galaxies. The properties of the emission-line spectra are presented and discussed in § 4. In § 5 these results are applied to the problem of measuring star formation rates in more distant galaxies.

2. OBSERVATIONS

The survey was carried out in two stages. Large-aperture, moderate-resolution (15–25 Å) spectrophotometry were obtained for 70 galaxies in 1985–1987, using the Intensified Reticon Scanner (IRS) on the 0.92 m telescope at Kitt Peak National Observatory (KPNO). This provided a basic set of continuum energy distributions and emission-line fluxes for a broad range of galaxy types. As this survey progressed, it became apparent that higher resolution and signal-to-noise ratio observations, sufficient to resolve the principal stellar absorption features and faint emission lines, would greatly enhance the value of the data base. Subsequently higher resolution (5–7 Å) data were obtained for 44 galaxies in 1989–1991, using the CCD spectrograph on the Steward Observatory 2.3 m telescope.

2.1. *Galaxy Sample*

In order to characterize the spectral properties of the Hubble sequence, objects covering the full range of morphological types were observed. These included galaxies with small angular diameters which could be adequately sampled with the 45″ apertures in the low-resolution survey (below), and larger galaxies which were observed with multiple apertures, or by drift-scanning the galaxies across a single aperture. High-resolution data with sufficient signal-to-noise ratio to measure the primary absorption features were obtained for at least three galaxies each of types E, S0, Sa, Sb, Sc, Im, and I0.

As demonstrated later, normal galaxies occupy only a small fraction of the observed range of spectral properties. Consequently a special effort was made to measure a diverse set of nearby emission line galaxies and other peculiar systems. Most were selected from the Huchra (1977) sample of star-forming Markarian galaxies. The remainder consist of interacting galaxies selected from the Hα survey of Kennicutt et al. (1987), and a few emission-line galaxies in the Abell 1367 and Coma Clusters, taken from the survey of Kennicutt, Bothun, & Schommer (1984). Additional spectrophotometry in the blue ([O II] λ3727, Hβ) is available for 75 blue galaxies from Gallagher et al. (1989).

Finally, a variety of galaxies with luminous active nuclei were included in the survey, in order to assess the effect of the nucleus on the integrated spectrum, and to test whether such objects can be readily distinguished from star-forming galaxies, when only an integrated spectrum is available. The sample included Seyfert 1 and 2 galaxies from the compilation of Weedman (1977), and galaxies with H II region–like starburst nuclei from Kennicutt, Keel, & Blaha (1989).

2.2. *Low-Resolution Spectra*

Spectra covering the range 3650–6900 Å were obtained for 70 galaxies during three observing runs in 1987–1989, using the dual beam IRS spectrometer on the KPNO No. 2 0.92 m telescope (f/7.5 focus). This instrument is well suited for measurements of extended objects, because its compact image scale and fast camera make it possible to obtain moderate resolution spectra with large entrance apertures.

Measurements were made with a pair of 45″.5 circular apertures, with centers separated by 61″.2 on an east-west line. True integrated spectra were only obtained for galaxies with diameters less than 45″. Most of the blue galaxies in the sample met this condition, but normal galaxies with this diameter are generally too faint ($B \simeq 14$–16) to measure on a 1 m telescope. Instead several galaxies with diameters of 45″–90″ (E-W) were observed, with the aperture covering the central 45″ region. In addition, 14 very large galaxies ($D = 2'$–$10'$) were observed in nebular mode, i.e., both apertures on object, with separate sky observations. Each galaxy was measured at two to five positions (pairs), usually spaced along an east-west line, and a pseudo-integrated spectrum was constructed by adding the individual spectra with appropriate weighting factors.

Each observation consisted of a series of integrations in alternating apertures, with the beam switching (or sky offsetting for nebular mode) performed under computer control. Total integration times were 4–180 minutes, depending on the brightness of the galaxy and the relative strengths of the emission lines. The data were taken in photometric or near-photometric conditions.

All galaxies were observed using a 500 gpm grating blazed at 5500 Å with a WG-360 UV-blocking filter, which provided photometric coverage over 370–6900 Å. With the large apertures, the spectral resolution was modulated by the luminosity distributions of the galaxies, ranging from 12 Å FWHM for a point source (such as an emission-line nucleus) to 25 Å for uniform illumination of the 45″ apertures. The actual resolution for most of the data is 15–20 Å FWHM. Additional observations in the blue (3600–5500 Å) were obtained for approximately half of the program galaxies, using a 400 gpm grating blazed at 800 Å in second order behind a $CuSO_4$ filter. This provided somewhat better resolution (typically 9–13 Å), and higher sensitivity shortward of 4000 Å.

The spectra were calibrated using standard techniques, and details can be found in Paper II. Special tests were made to verify the uniformity of response over the large-entrance apertures. The overall accuracy of the spectrophotometry is estimated to be approximately ±5%–10%, based on comparison of independent measurements of the same objects with different configurations, and comparisons with published scanner observations. The largest sources of error are crosstalk between the two Reticon channels, caused by scattered light in the IRS (Barnes, Massey, & Carder 1986), combined with uncertainties of a few percent in the spectrophotometric calibration.

2.3. *High-Resolution Spectra*

The degradation of spectral resolution with increasing slit width is a severe limitation for fixed pointing observations of galaxies with large angular diameters. To solve this problem, a drift scanning technique was used to obtain higher resolution (5–7 Å) data for 44 galaxies with diameters of 1′–14′. The spectra were obtained using the Boller & Chivens (B&C) CCD spectrograph on the Steward Observatory 2.3 m telescope, over 10 nights in 1989–1991. Each measurement consisted of one or more integrations, during which the image of the galaxy was trailed across a long slit several times. The spectral resolution was dictated by the slit width, while the aperture on the sky was defined by the slit length in one direction, and the length of the drift scan in the perpendicular direction.

The B&C spectrograph was used with a thinned 800 × 800 TI CCD, which was UV-flooded for enhanced blue response. Two grating settings were used to cover the full visible spectrum. A 600 gpm grating blazed at 3568 Å covered the 3650–5150 Å region, and a 400 gpm grating blazed at 7500 Å (with 4200 Å blocking filter) covered the 4950–7150 Å region. The blue and red spectra were tied together by normalizing the mean fluxes in the 4950–5150 Å overlap region, or by normalizing the respective fluxes in the [O III] λ5007 emission line. A 2.″5 slit yielded a resolution of 4.5 Å in the blue and 7 Å in the red. The usable slit length was roughly 3.′5 and included the program galaxies ($D_{proj} \leq 2.'5$) and adjacent sky. Several larger, inclined galaxies were measured by aligning the slit with the minor axis, and drift-scanning the telescope along the major axis. Drift rates were adjusted so that the image crossed the slit at least four times, to minimize errors due to small variations in drift speed or transparency. Integration times were 20–60 minutes and were of sufficient length to ensure that sky noise dominated over chip-read noise in all cases.

Data reduction followed standard techniques, using the CCDRED and LONGSLIT packages in the IRAF software package. Each observation produced a two-dimensional spectrum, but since the telescope was drifted during the exposure, most true spatial information is lost. Consequently the data were summed into one or more one-dimensional, sky-subtracted spectra. The accuracy of the spectrophotometry was evaluated internally using residuals of the standard star calibrations and externally by comparing the galaxy energy distributions to IRS observations in common, and to published multichannel scanner observations. These tests show that the spectrophotometry is accurate to better than ±5% over small wavelength regions, and about ±10%–15% or better on large scales. The errors are dominated by the accuracy of the sky subtraction. Crinkling of the thinned CCD detector introduces small variations in line position and width along the slit, and this mainly affects the sky subtraction near strong night sky emission lines. A detailed discussion of the spectrophotometric accuracy is given in Paper II.

2.4. *Emission-Line Measurements*

Acceptable quality spectrophotometry was obtained for a total of 90 galaxies, including 24 with both high- and low-resolution spectra. Of these, 80 possessed measureable emission lines, and the remainder of this paper deals with the properties of that subsample.

The equivalent widths (EWs) and fluxes of the emission lines were measured by direct numerical integration, using the SPLOT program in IRAF. The continuum levels and integration limits for the lines were set interactively, with repeat measurements made in difficult cases. Galaxies with weak emission lines were measured with the IRS at least once at each dispersion, to provide two independent measurements and a direct evaluation of the observational uncertainties. Lines measured included the Hα + [N II] λλ6548, 6583 blend, Hβ, [O II] λ3727, [O III] λ5007, and when available [S II] λλ6717, 6731. In most cases the Hα and [N II] lines could be measured separately, by using the Gaussian deblending program in the SPLOT package. In addition a continuum "41–50" color index was measured by measuring the mean continuum intensities at rest wavelengths of 4050–4250 and 4900–5100 Å:

$$41\text{–}50 \equiv 2.5 \log \frac{f_\nu(5000)}{f_\nu(4100)} . \quad (1)$$

A complete listing of the emission-line data is given in Tables 1 and 2. Columns (1) and (2) list the galaxy name and Hubble type. The latter was taken from Sandage & Tammann (1981), de Vaucouleurs, de Vaucouleurs, & Corwin (1976), or Huchra (1977). Column (3) lists the aperture size in arcseconds, the diameter for a circular aperture, and EW × NS for nebular or drift-scanned observations. Column (4) lists the 41–50 continuum color as defined above. Equivalent widths for the primary emission features are given in columns (5)–(9), as defined above. The respective line fluxes, normalized to Hα + [N II] (except for [N II] λ6583/Hα), are listed in columns (10)–(14). Remarks are given in column (15).

The random errors in these data are dominated by shot noise and sky subtraction, with uncertainties ranging from about ±5%–10% in bright galaxies to ±30% in the weakest lines (3 σ) measured. In addition, a number of subtle systematic effects were encountered, and these merit further discussion, as they may be important sources of error in other spectroscopic surveys of galaxies.

The largest systematic effects are caused by superposed stellar absorption features, especially for the Balmer lines. In high-resolution spectra, the broad stellar absorption lines can be easily seen surrounding the narrow emission lines, but in low-resolution data, the components are blended, and one measures a weaker emission line, or no emission at all. Since a primary objective of this study is to aid in the interpretation of spectra of distant galaxies, which are usually obtained at low resolution and signal/noise, the line fluxes and EWs reported here refer to the raw data, including any superposed absorption. The effects of this absorption on the Balmer line measurements will be discussed in detail in § 3.

Another systematic problem is the nonlinear effect of spectral resolution on the detection and measurement of weak lines. All of the emission lines are superposed on a choppy absorption spectrum, and measuring errors increase rapidly when the line EWs became much smaller than the spectral resolution, or comparable to the strengths of adjacent absorption features. This effect was analyzed quantitatively in two ways. In one experiment, the fluxes of each of the components of the [O III] λλ4959, 5007 doublet were measured from the low-resolution IRS survey, and the observed 4959/5007 ratio (theoretical value 0.33) was plotted against the EW of the weaker line. At high signal-to-noise ratio, this ratio showed the expected uncertainty, but for EW(4959) ≤ 5 Å the errors in the doublet ratio increased dramatically, and deviated systematically from the theoretical value. The same effect was simulated by smoothing high resolution spectra to effective resolutions of

TABLE 1

HIGH-RESOLUTION DATA

				Equivalent Width (Å)					Flux (Hα + [N II] = 1)					
Name (1)	Type (2)	Aperture (3)	41–50 (4)	[O II] (5)	Hβ (6)	[O III] (7)	Hα + [N II] (8)	[S II] (9)	[O II] (10)	Hβ (11)	[O III] (12)	[S II] (13)	[N II]/Hα (14)	Notes (15)
NGC 488	Sab	120″ × 180″	0.77	2	−4	<0.5	2	...	0.45	...	...	...	1.72	
NGC 1357	Sa	120 × 90	0.64	4	−2.5	<0.3	9	1.5	0.18	...	<0.05	0.19	0.66	
NGC 1569	Sm/Im	120 × 60	0.66	49	35	182	202	25	0.13	0.16	0.91	0.13	0.66	
NGC 1832	SBb	90 × 90	0.43	17	0	2	34	7	0.34	0.02	0.07	0.21	0.43	
NGC 2276	Sc	120 × 120	0.26	33	7	10	84	21	0.39	0.10	0.15	0.25	0.30	
NGC 2775	Sa	90 × 90	0.87	1.6	−4	<0.5	2	...	0.3	...	...	...	0.81	
NGC 2798	Sap	60 × 90	0.54	17	1	3	53	11	0.18	0.02	0.05	0.21	0.27	1, 2
NGC 2799	Sm	40 × 90	0.46	26	7	5	53	13	0.39	0.10	0.12	0.24	0.28	1
NGC 2903	Sc	150 × 360	0.46	8	−1.5	<0.6	28	5	0.17	...	<0.02	0.17	0.47	
NGC 3034	I0	314 × 120	0.57	7	−3.5	1.5	45	9	0.06	...	0.03	0.17	0.58	3
NGC 3077	I0	120 × 120	0.43	22	2	5	38	8	0.37	0.07	0.14	0.21	0.27	
NGC 3147	Sb	120 × 120	0.69	3	−1	<0.5	11	...	0.13	...	...	...	0.47	
NGC 3227	Sb	120 × 80	0.60	10	...	7	32	5	0.14	...	0.21	0.17	...	4
NGC 3310	Sbcp	90 × 65	0.15	63	20	48	153	34	0.73	0.20	0.46	0.22	0.21	
NGC 3368	Sab	120 × 180	0.77	4	−3.5	<0.5	4	1.5	0.36	...	...	0.34	1.35	
NGC 3516	S0	60 × 60	0.77	7	7	13	63	6	0.08	0.10	0.22	0.09	...	4
NGC 3623	Sa	90 × 600	0.72	1.5	−3	<0.5	2.4	1	0.2	...	...	0.3	2.4	
NGC 3627	Sb	150 × 180	0.49	5	−3	<0.4	20	4	0.16	...	<0.02	0.20	0.46	
NGC 3921	S0p	60 × 45	0.60	11	−3	<0.5	15	...	0.30	...	<0.03	...	0.77	
NGC 4449	Sm/Im	180 × 120	0.25	55	11	33	84	21	0.97	0.19	0.57	0.25	0.12	3
NGC 4485	Sm/Im	90 × 90	0.29	48	4	33	65	15	1.07	0.12	0.75	0.22	0.10	1
NGC 4631	Sc	800 × 110	0.33	40	4	15	60	18	0.79	0.09	0.36	0.31	0.21	
NGC 4670	SBp	60 × 45	0.30	62	22	54	114	26	0.75	0.25	0.66	0.11	0.22	
NGC 4750	Sbp	90 × 45	0.67	5	−2	<0.5	16	3	0.17	...	<0.03	0.18	0.54	
NGC 4775	Sc	90 × 90	0.28	35	6	14	56	17	0.90	0.16	0.35	0.29	0.22	
NGC 5195	I0p	90 × 90	0.96	7	−5	<0.5	3.5	2	0.52	...	0.06	0.47	10.3	1
NGC 5248	Sbc	150 × 180	0.48	9	1	1	31	6	0.17	0.03	0.03	0.18	0.42	
NGC 5548	S0/a	60 × 45	0.53	6	10	26	113	...	0.05	0.12	0.26	...	...	4
NGC 6181	Sc	90 × 60	0.53	15	1.5	3.5	47	10	0.22	0.03	0.07	0.21	0.41	
NGC 6217	SBbc	90 × 90	0.55	12	0	2	40	8	0.26	...	0.06	0.21	0.53	
NGC 6240	I0p	40 × 45	0.75	67	3	11	104	31	0.27	0.02	0.10	0.31	>1	5
NGC 6643	Sc	120 × 90	0.52	11	0	1.5	35	8	0.22	...	0.05	0.21	0.38	
NGC 7714	Sp	60 × 45	0.26	59	22	46	172	30	0.65	0.14	0.34	0.21	0.23	1, 2
UGC 6697	Sp	120 × 20	0.19	44	8	22	77	18	0.65	0.14	0.34	0.21	0.23	3, 6
Mrk 3	S0	60 × 45	0.92	150	16	157	147	39	0.27	0.10	0.92	0.26	...	4
Mrk 270	S0	60 × 45	0.95	33	0.5	20	17	7	0.64	0.03	1.13	0.41	0.90	4

NOTES.—(1) Strongly interacting galaxy. (2) Contains starburst nucleus. (3) Long aperture dimension along major axis of galaxy. (4) Contains Seyfert nucleus. (5) Peculiar galaxy, probable merger. (6) Member of Abell 1367 cluster.

7–30 Å and remeasuring the EWs and fluxes of the emission lines. Strong emission lines (EW ≥ 30 Å) were essentially unaffected by the degraded resolution, while very weak lines (few Å EW) were completely lost when the resolution exceeded the EW by factors of a few. At intermediate resolution the errors in line fluxes increased rapidly as resolution was degraded, and the mean ratios sometimes deviated systematically from the true value, depending on whether the lines fell near strong absorption features.

Spatial undersampling of the larger galaxies by the 45″ IRS apertures was another potential source of error. We tested the importance of this effect by observing several large galaxies with both the IRS (central 45″ only) and the 2.3 m telescope (full spatial coverage). In most cases the line fluxes and EWs measured in the IRS aperture were representative of the integrated spectrum, outside of an absolute scale factor, but in several of the Sb-Sc galaxies the emission lines were systematically weaker in the IRS spectra. This mainly occurs because continuum emission (from a disk and bulge) is more centrally concentrated than the nebular disk emission in many galaxies. This undersampling tends to reduce the strengths of all of the emission lines in roughly equal proportion (with the possible exception of [O III]), so the relative line fluxes in Table 2 should be relatively insensitive to these aperture effects. Nevertheless, the absolute values of emission-line EWs can be strongly affected, and for this reason observations which might be seriously influenced by undersampling were removed from the sample, and do not appear in Table 2. Borderline cases are noted in Table 2.

Taken together, these systematic effects can qualitatively alter the character of a galaxy spectrum. As an example, Figure 1 shows two spectra of the same Sc galaxy, NGC 6181, observed at 5–7 Å resolution on the 2.3 m telescope (90″ × 60″ aperture), and at 20 Å resolution with the IRS scanner (45″ aperture). The strong Hα + [N II] feature shows up prominently in both spectra, but the weaker lines such as Hβ and [O III] are virtually lost in the IRS spectrum. The difference is due to a combination of undersampling of the disk in the 45″ IRS aperture, and blending of weak lines at low spectral resolution. In Sa–Sb galaxies, the effects are even stronger. This illustrates that high spectral resolution and adequate aperture coverage are imperative for the study of normal galaxies (type Sc and earlier) at any redshift.

3. GENERAL SPECTRAL CHARACTERISTICS OF GALAXIES

Before discussing the quantitative properties of the emission-line spectra, it is useful to examine the general variation in spectra along the Hubble sequence, and among various

TABLE 2

LOW-RESOLUTION DATA

				Equivalent Width (Å)					Flux (Hα + [N II] = 1)					
Name (1)	Type (2)	Aperture (3)	41–50 (4)	[O II] (5)	Hβ (6)	[O III] (7)	Hα + [N II] (8)	[S II] (9)	[O II] (10)	Hβ (11)	[O III] (12)	[S II] (13)	[N II]/Hα (14)	Notes (15)
NGC 2798	Sap	45″	0.55	12	4	2	68	11	0.08	0.04	0.02	0.16	0.44	1, 2
NGC 2841	Sb	110 × 165	0.95	<1	−1.5	...	1.5	...	<0.2	...	...	...	...	3, 4
NGC 2881	S	45	0.33	29	8	8	54	...	0.52	0.16	0.16	...	...	1
NGC 3303	P	45	0.87	35	−3	2	17	4	0.6	...	0.12	0.3	...	5
NGC 3310	Sbcp	45	0.09	58	17	51	161	33	0.58	0.16	0.44	0.19	0.26	
NGC 3395	Scd	45	0.12	44	11	23	92	32	0.64	0.16	0.32	0.33	0.18	1
NGC 3516	S0	45	0.76	8	...	19	61	6	0.06	...	0.33	0.11	...	6
NGC 3690	Scp	45	0.30	48	22	30	234	50	0.18	0.10	0.14	0.21	0.39	1
NGC 3991	Im	45	0.07	60	21	65	155	33	0.73	0.21	0.62	0.22	0.15	1
NGC 3994	Scp	45	0.48	36	5	6	73	16	0.33	0.06	0.08	0.22	...	1
NGC 3995	Smp	45	0.17	43	11	25	92	31	0.61	0.17	0.37	0.33	0.20	1
NGC 4156	SBc	45	0.60	10	1	<1	24	...	0.22	0.03	<0.03	...	0.69	
NGC 4449	Sm/Im	110 × 165	0.28	40	10	30	71	16	0.57	0.19	0.57	0.22	...	3, 4
NGC 4631	Sc	170 × 45	0.36	24	2	9	41	13	0.37	0.05	0.27	0.32	...	3, 4
NGC 4670	SBp	45	0.22	62	23	67	134	41	0.65	0.22	0.65	0.30	0.11	
NGC 4704	SBc	45	0.53	12	−1	1	24	...	0.27	...	<0.04	...	0.64	
NGC 4736	Sab	230 × 45	0.73	2	−2	...	7	2	0.18	...	<0.1	0.27	...	4
NGC 4826	Sab	170 × 45	0.76	<2	−2	...	5	1	<0.2	...	<0.1	0.2	...	4
NGC 4848	Sc	45	0.47	25	4	4	54	5	0.36	0.08	0.08	...	0.53	7
NGC 4900	Sc	45	0.38	18	1	<1	42	9	0.34	0.02	<0.03	0.20	...	8
NGC 5055	Sbc	230 × 45	0.67	4	−1	...	15	2	0.11	...	<0.02	0.13	...	4
NGC 5194	Sbc	105 × 165	0.55	5	1	...	34	5	0.08	0.02	<0.01	0.14	...	4
NGC 5548	S0/a	45	0.44	4	47:	33	203	...	0.02	0.22	0.16	...	...	6
NGC 5929	Sbcp	45	0.78	40	0	12	29	12	0.25	...	0.34	0.45	0.55	1, 6
NGC 5953	Sap	45	0.56	13	1	6	54	10	0.13	0.02	0.10	0.20	0.56	1, 6
NGC 5954	Scdp	45	0.47	22	4	2	73	13	0.23	0.06	0.03	0.18	0.39	1
NGC 6240	I0p	45	0.63	77	0	11	126	34	0.22	<0.01	0.08	0.28	...	5
NGC 6764	SBb	45	0.58	45	5	7	86	20	0.27	0.05	0.08	0.24	0.88	6
NGC 7448	Sc	45	0.36	23	2	6	51	14	0.33	<0.04	0.13	0.21	...	8
NGC 7469	Sa	45	0.41	8	21	21	143	13	0.06	0.16	0.16	0.1	0.68	1, 6
NGC 7714	Sp	45	0.34	76	22	41	196	35	0.40	0.13	0.26	0.17	0.37	1, 2
IC 883	Im	45	0.34	23	−5	3	22	...	0.6	...	<0.14	...	1.02	1, 5
IC 1236	Sc	45	0.47	10	1	<2	33	9	0.21	<0.03	<0.06	0.3	0.38	
UGC 6697	Sp	45	0.37	36	11	14	69	32	0.56	0.19	0.27	0.47	0.32	9
Z130–008	Im	45	...	16	2	6	65	...	0.24	0.04	0.12	...	0.35	9
Mrk 33	Im	45	0.24	62	21	43	156	26	0.55	0.17	0.35	0.17	0.22	
Mrk 35	Im	45	0.21	85	28	115	167	23	0.63	0.22	0.86	0.14	0.12	
Mrk 59	Im	45	...	62	115	750	796	86	0.29	0.28	1.65	0.09	0.04	10
Mrk 71	Im	45	...	108	299	2490	1350	61	0.17	0.31	2.00	0.04	0.02	10
Mrk 111	Im	45	0.25	60	15	43	148	40	0.41	0.12	0.35	0.25	0.16	
Mrk 158	Sab	45	0.54	11	0	<2	32	9	0.19	...	<0.06	0.26	0.48	
Mrk 161	SBc	45	0.30	21	4	4	81	...	0.24	0.06	0.06	...	0.51	
Mrk 181	SBc	45	0.28	28	10	12	92	37	0.35	0.16	0.18	0.38	0.40	9
Mrk 188	Sc	45	0.46	15	0	1	41	7	0.22	...	<0.03	0.18	0.45	
Mrk 201	Smp	45	0.35	36	11	14	124	21	0.25	0.10	0.13	0.18	0.49	
Mrk 256	Sd	45	0.13	47	17	30	115	30	0.53	0.22	0.40	0.27	0.35	
Mrk 270	S0	45	0.98	28	<1	22	18	...	0.40	0.14	0.39	0.23	0.21	6
Mrk 286	Scd	45	0.23	24	4	9	83	...	0.23	0.06	0.13	...	0.45	
Mrk 296	Im	45	0.17	91	27	57	103	...	1.2:	0.38:	0.81:	...	...	
Mrk 297	Smp	45	0.17	54	20	53	181	46	0.40	0.14	0.39	0.23	0.21	1
Mrk 432	SBdmp	45	0.23	43	10	17	94	37	0.36	0.12	0.21	0.39	...	
Mrk 479	SBc	45	0.28	27	7	9	72	10	0.32	0.13	0.16	0.15	0.26	
Mrk 487	Im	45	−0.14	50	70	304	160	30	0.51:	0.4:	1.78:	0.15:	...	
Mrk 685	Sc	45	0.19	99	19	79	131	23	1.08	0.23	0.95	0.16	0.14	
Mrk 691	SBd	45	0.19	24	11	11	93	24	0.27	0.15	0.17	0.27	0.36	

NOTES.—(1) Strongly interacting galaxy. (2) Contains starburst nucleus. (3) Long-aperture dimension along major axis of galaxy. (4) Observed in nebular mode. (5) Peculiar galaxy, probable merger. (6) Contains Seyfert nucleus. (7) Member of Coma Cluster. (8) Data may be influenced by spatial undersampling; see text. (9) Member of Abell 1367 cluster. (10) Aperture centered on dominant H II region in large galaxy.

types of peculiar galaxies. Several examples are illustrated in Figures 2–3. A more complete library is presented in Paper II.

3.1. *Normal Galaxies*

Figure 2 illustrates the progression of integrated spectra along the Hubble sequence. These data were obtained with the 2.3 m telescope, with resolutions of 4.5–5 Å in the blue and 7–8 Å longward of 5100 Å, and smoothed with a 4 Å square filter. Table 3 summarizes the main properties of these galaxies (assuming $H_0 = 75$ km s^{-1} Mpc^{-1}). Two versions of each spectrum are plotted. Figure 2*a* shows the full spectral coverage, with the different spectra scaled to roughly the same peak intensity. Figure 2*b* shows expanded plots of the region blueward of 5500 Å. In both cases the ordinate shows the flux

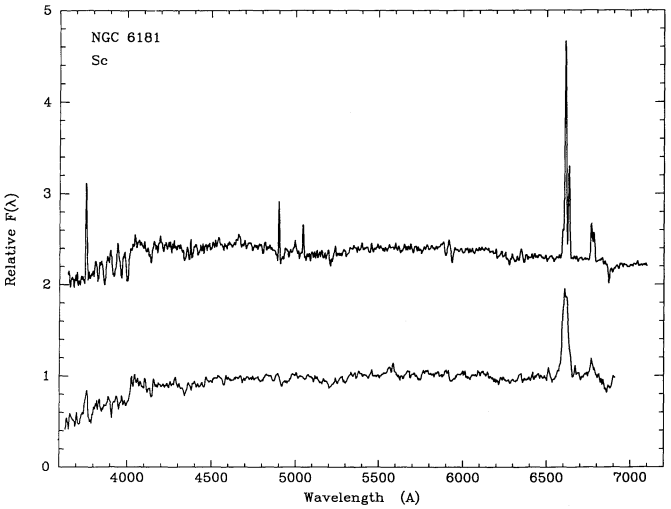

FIG. 1.—Comparison of two spectra of NGC 6181, showing the effects of resolution and spatial sampling. The top spectrum was obtained by drift-scanning a narrow slit over a 90″ × 60″ region. Resolution is 5–7 Å. The bottom spectrum is a single pointed observation of the central 45″, with roughly 20 Å resolution.

normalized to unity at a reference wavelength of 5500 Å. The spectra are corrected for atmospheric extinction but are uncorrected for Galactic or intrinsic reddening. Residual features from bright night sky lines (mainly [O I] λ5577, 6300, 6364) have been clipped for clarity, unless the night sky artifact fell near a real spectral feature in the galaxy (e.g., Na D at low redshift).

The integrated spectra follow the general patterns discussed originally by Morgan & Mayall (1957) and Morgan & Osterbrock (1969). Elliptical and S0 galaxies (NGC 4889, 4262) are dominated by absorption features. NGC 4889 shows no detectable emission lines at all, but faint [O II] and [N II] lines, with EWs in the range 0.3–3 Å, are detected in many of the E/S0 galaxies, including NGC 4262. Balmer emission may be present as well, but it is almost always lost in the stellar absorption in the integrated spectra. Note that the choppy continuum structure is real, produced in large part by blended stellar absorption lines in the K giant dominated continuum.

Spectra of the nuclear regions of E–S0 galaxies have been studied extensively for spectral synthesis applications, and the integrated spectra obtained here are very similar (e.g., Pickles & Visvanathan 1985). While the strengths of metal-sensitive features such as Mg b and Na D tend to be somewhat weaker in the integrated spectra, the EW of the metallicity-insensitive Ca II (H+K) doublet is virtually constant over our sample, with the same mean EW as the nuclei studied by Pickles & Visvanathan (1985). This lends some support for the efficacy of our sky subtraction and reduction procedures. Further discussion of the absorption spectra is deferred to future papers.

TABLE 3

PROPERTIES OF GALAXIES ILLUSTRATED IN FIGURES 2 AND 3

Name	Figure	Type	$M(B)$	Remarks
NGC 4889	2	E4	−22.1	Coma Cluster
NGC 4262	2	SB0	−18.4	
NGC 2775	2	Sa	−19.9	
NGC 4750	2	Sb	−20.2	
NGC 6181	2	Sc	−20.7	
NGC 4449	2	Sm	−17.9	
NGC 3516	3	SB0	−20.6	Seyfert 1
Mrk 270	3	S0	−18.5	Seyfert 2
NGC 3310	3	Sbcp	−19.9	Global starburst
NGC 7714	3	Sdmp	−19.7	Nuclear starburst
NGC 3034 (M82)	3	I0	−18.5	IR luminous
NGC 6240	3	I0	−21	IR luminous, merger

The spectra of early-type spirals, such as NGC 2775 (Sa), are also dominated by late-type stars and differ only subtly from the spectra of E–S0 galaxies. The main changes are an increase in the blue continuum, seen most easily as a decrease in the strength of the 4000 Å H+K break, and the appearance of weak Hα and [N II] emission, at the level of a few Å or less in EW. Except for occasional weak [O II] emission, no other nebular lines are detected in the integrated spectrum. Exceptions are invariably galaxies with active nuclei, such as Seyfert or starburst galaxies.

Intermediate- to late-type spirals, illustrated by NGC 4750 (Sb) and NGC 6181 (Sc), are characterized by much bluer continua, more prominent Balmer absorption lines, and nebular emission lines. Hα and [N II] remain the dominant emission features, but lines at (in descending order) [S II], [O II], Hβ, and [O III] begin to appear. As one progresses to the bluest spirals and Magellanic irregulars, as illustrated by NGC 4449 (SBm/Im), the integrated spectrum becomes increasingly dominated by the continua of B–A stars, and by strong nebular emission lines. The smooth monotonic progression in both the emission and absorption spectra with galaxy type (compare Figs. 2*a* and 2*b*) shows clear evidence of the systematic changes in stellar populations and star formation rates along the Hubble sequence.

Although the character of the integrated spectrum changes radically over the range of the Hubble sequence, the most revealing result in Figure 2 is the subtlety of the changes in composite spectrum between Hubble types E and Sb. Most of the variance in spectral properties, especially in the blue region, occurs among Sc–Irr galaxies. The sole exception is the Hα + [N II] emission feature, which is sensitive to stellar population over the entire range of types; it is not surprising why Hα is used for quantitative measurements of star formation rates in galaxies! This is in marked contrast to the remainder of the spectrum. If observed shortward of Hα at moderate spectral resolution (≥10 Å), typical parameters for faint galaxy surveys, the spectra of galaxies ranging in type from E to early Sc are nearly indistinguishable from qualitative inspection alone. Only a precise (~10%) measurement of the continuum shape shortward of 4500 Å, or high-resolution observations of the [O II] line would suffice to characterize the stellar population or galaxy type within this range. Conversely, any galaxy which does exhibit a prominent emission-line spectrum in the blue almost certainly will be a peculiar galaxy, with abnormally high levels of star formation and/or nuclear activity.

In general the spectral sequence shown in Figure 2 closely parallels the Yerkes spectral classification (Morgan 1958), except that the best-fitting spectral types here tend to be somewhat earlier (i.e., earlier mean *stellar* type) than on the Yerkes system. This difference can be attributed entirely to the fact that the Morgan types were based on spectra which primarily sampled the nuclear regions, whereas here integrated spectra are available. In most normal galaxies (excluding Seyfert and extreme starburst galaxies) the nuclear regions contribute only a few percent or less of the integrated flux, in either the continuum or the emission lines (Kennicutt & Kent 1983), so in most cases the spectral appearance is dominated by the disk and

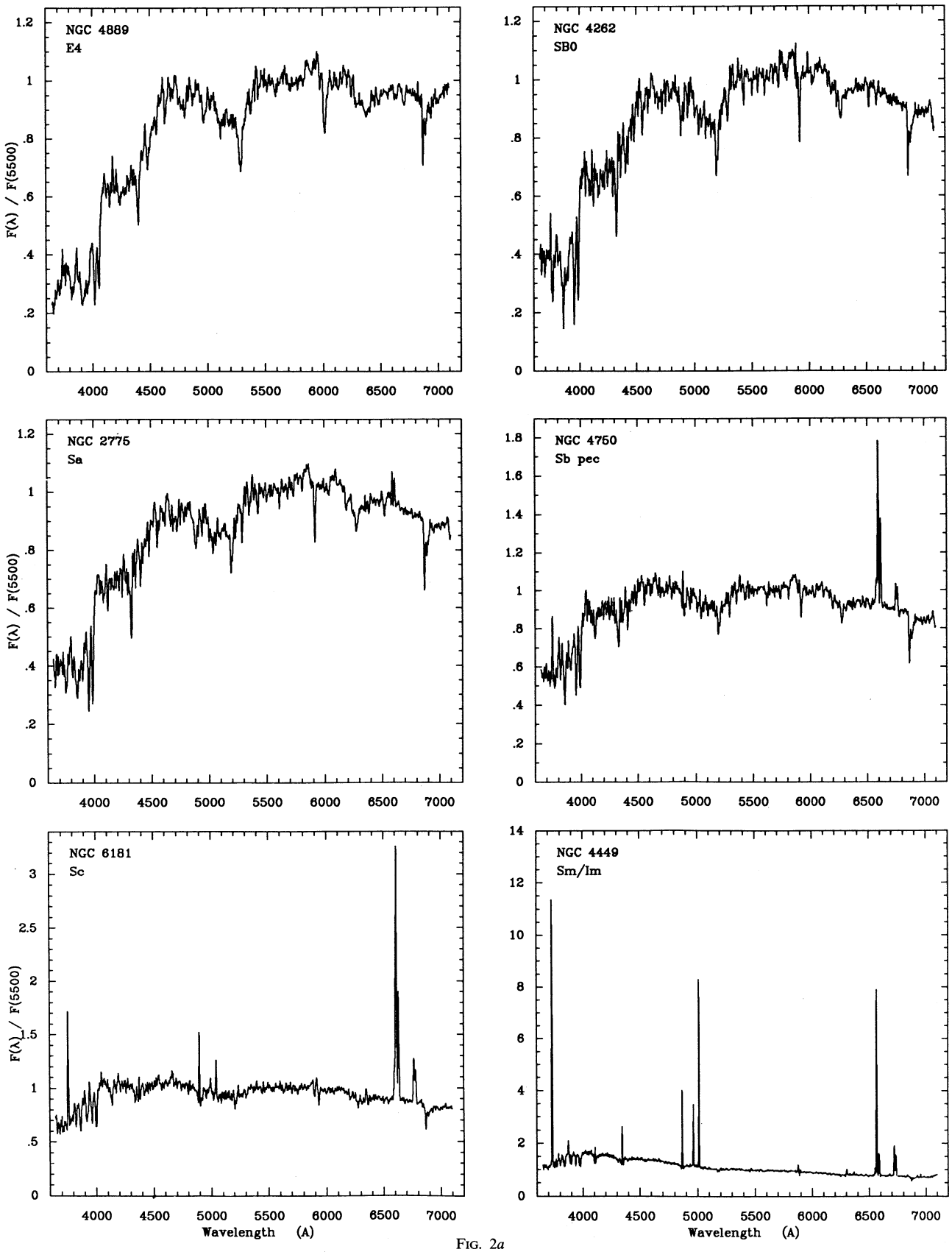

FIG. 2a

FIG. 2.—(*a*) The spectral Hubble sequence. Galaxies are shown in order of increasing Hubble type from top to bottom. See Table 3 for data on the galaxies. (*b*) Same spectra as in (*a*), but expanded in the blue to show the properties of the absorption-line spectra.

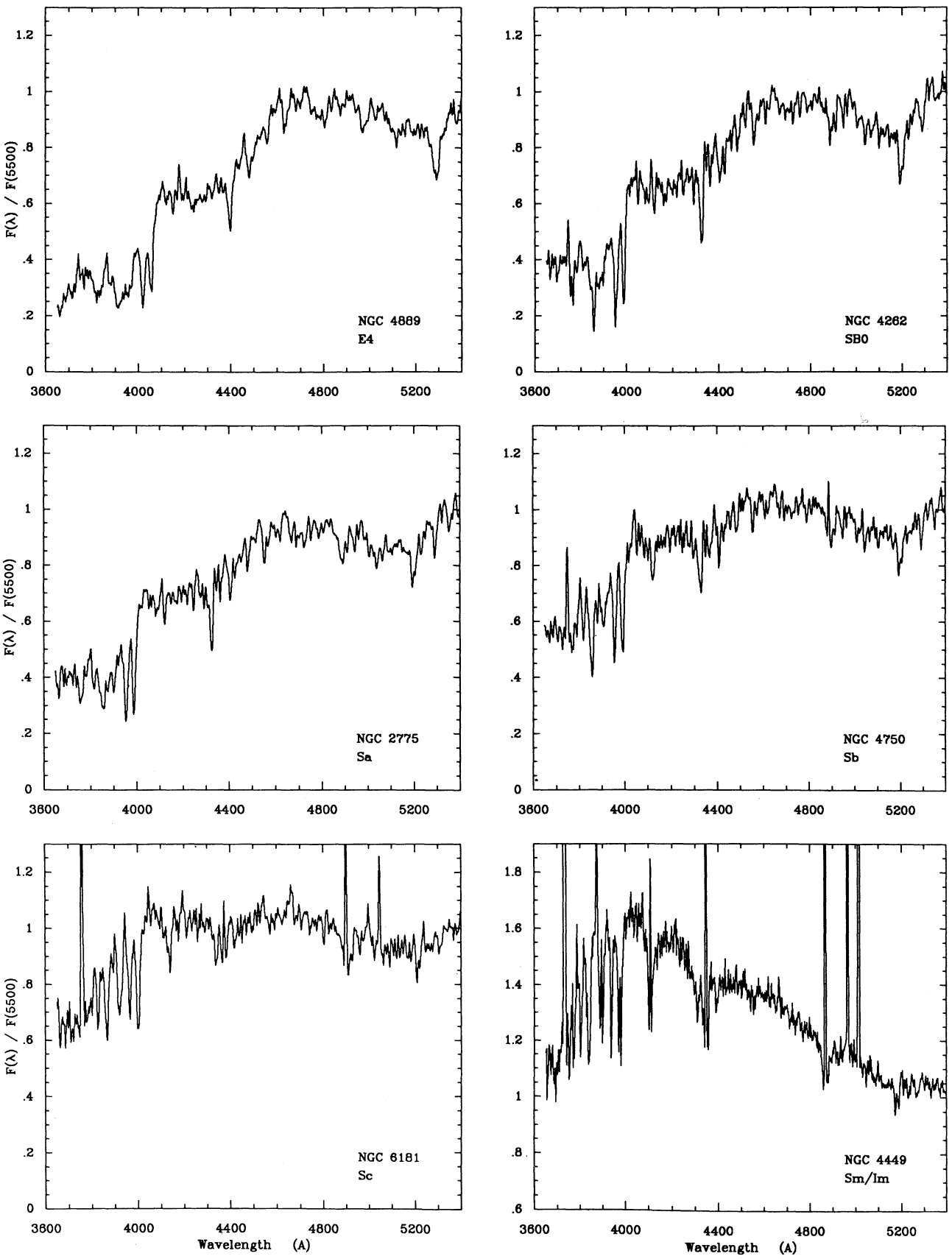

FIG. 2*b*

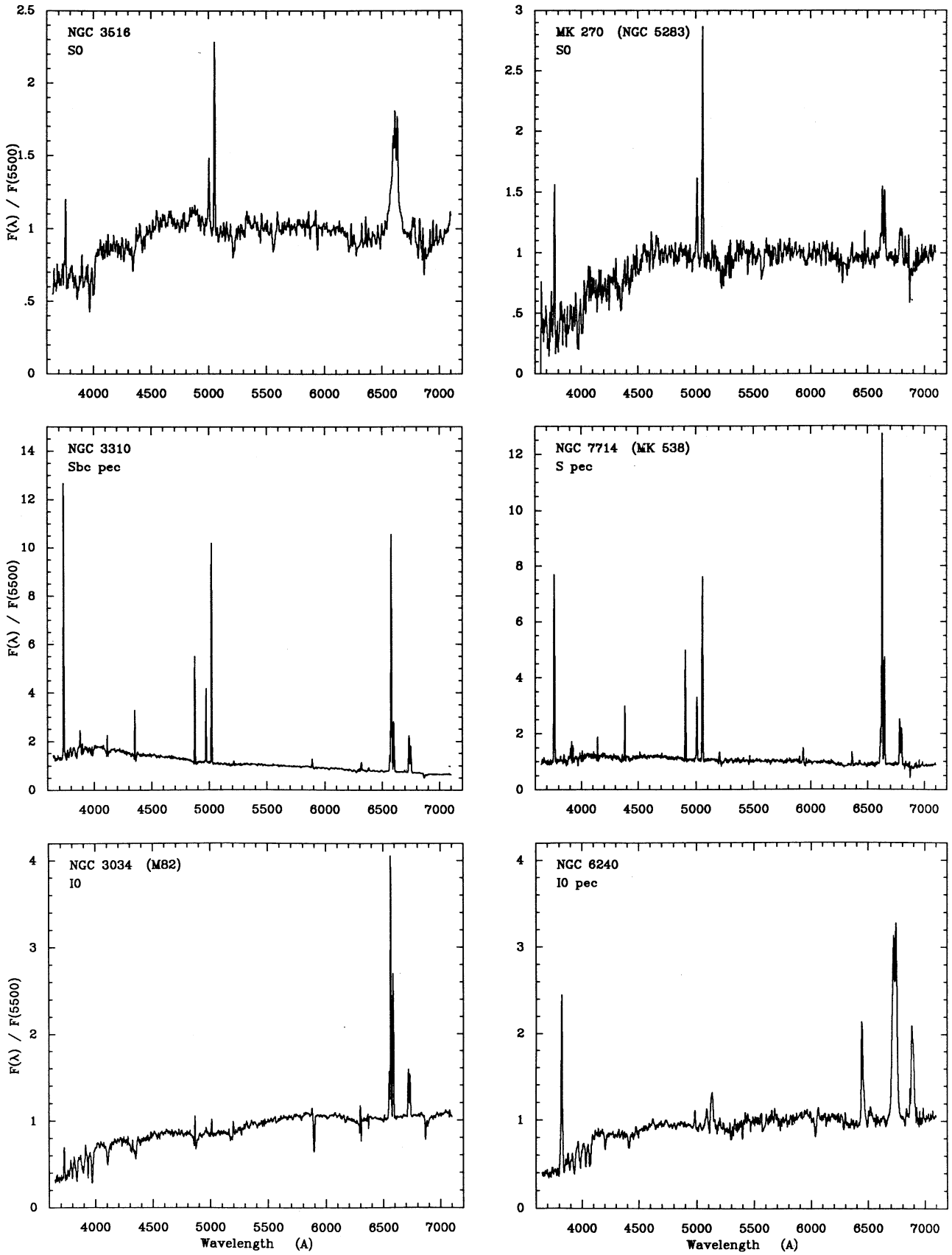

FIG. 3*a*

FIG. 3.—(*a*) Spectra for six peculiar galaxies with active nuclei or star formation bursts. Note that the spectral resolution changes shortward and longward of 5200 Å, so relative line strengths cannot be inferred directly from the plots. See Table 3 for data on galaxies. (*b*) Same spectra as in (*a*), but expanded in the blue to show the properties of the absorption-line spectra. For clarity the spectra have been aligned in wavelength.

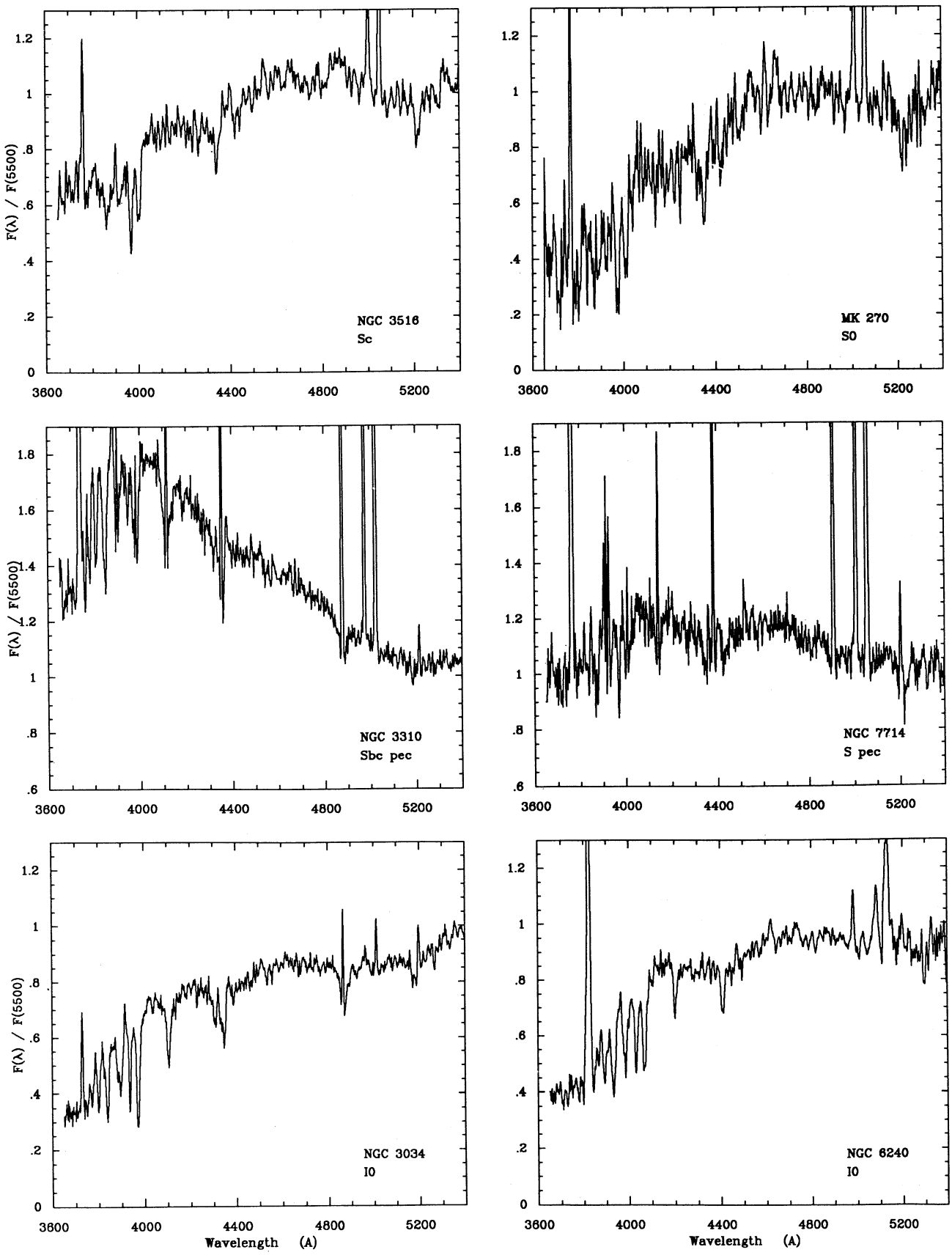

FIG. 3*b*

bulge. On the other hand, the apertures used in this study generally did not extend to the faintest isophotes (A/D_{25} = 0.5–1.2 in most cases), so the spectra may be slightly biased to the highest surface brightness regions. The galaxy sample also is underrepresented in very low surface brightness galaxies, so the conclusions of this paper may not necessarily apply to those objects.

3.2. *Galaxies with Peculiar Spectra*

Figures 3*a* and 3*b* show spectra of several peculiar galaxies, again in full scale and expanded form, respectively. The properties of these galaxies are listed in Table 3. The Seyfert galaxies NGC 3516 (Sy 1) and Mrk 270 (Sy 2) are clearly recognizable as such, even in an integrated spectrum. Data obtained for several other Seyfert galaxies (Paper II) show that identification of luminous Seyfert 1 nuclei is usually straightforward, due to the unmistakable broad Balmer emission lines, but recognizing a Seyfert 2 nucleus in the integrated spectrum is often more difficult. The latter are usually identified on the basis of an abnormally high [O III]/Hβ ratio (e.g., Baldwin, Phillips, & Terlevich 1981; Dressler & Gunn 1983; Dressler et al. 1985), but high-excitation star-forming galaxies can mimic this spectrum, especially when strong Balmer absorption is superposed. Various quantitative means for distinguishing the two types of galaxies are discussed in § 4.4.

NGC 3310 and NGC 7714 are examples of starburst emission-line galaxies. Most of the blue galaxies in our Markarian sample fall into this category, with an emission spectrum characteristic of moderate to high-excitation H II regions, and line EWs of order 10–100 Å. NGC 3310 is an example of a galaxy with a global disk star formation burst, while NGC 7714 is the prototypical example of a nuclear starburst galaxy. The emission-line ratios for the nuclear and disk starbursts are very similar (Kennicutt et al. 1989), so it is virtually impossible to distinguish between the two classes from integrated spectra alone.

Finally, Figure 3 displays spectra of two peculiar irregular galaxies, NGC 3034 (M82) and the infrared-luminous galaxy NGC 6240. M82 exhibits strong line emission and a heavily reddened continuum dominated by Balmer absorption lines. Note the unusually strong Na D absorption, which is probably interstellar in origin. The spectrum of NGC 6240 is extremely peculiar, with abnormally strong and broad lines of [O I] λ6300 and [S II] $\lambda\lambda$6717, 6731. The absorption spectrum, on the other hand, is fairly typical of a normal late-type, actively star-forming galaxy (cf. Fig. 2).

4. EMISSION-LINE SPECTRA AND STAR FORMATION DIAGNOSTICS

For ionization-bounded H II regions, the Balmer emission-line luminosities scale directly with the ionizing fluxes of the embedded stars, and this makes it possible to use the Balmer lines to derive quantitative star formation rates (SFRs) in galaxies (e.g., Kennicutt 1983; Gallagher, Hunter, & Tutukov 1984). Inspection of Figure 2 shows that Hα is clearly the best line for such applications, but beyond $z \simeq 0.2$–0.3, Hα redshifts into the near infrared, and for many applications it becomes more practical to measure the emission lines in the blue.

Several workers have applied the EW of the [O II] λ3727 doublet as a star formation index for distant galaxies (e.g., Dressler & Gunn 1982; Dressler et al. 1985; Peterson et al. 1986; Broadhurst et al. 1988; Lavery & Henry 1988; Colless et al. 1990). Gallagher et al. (1989) have derived an approximate [O II] versus SFR calibration from observations of [O II] and Hβ in a nearby blue galaxies. In this section we extend that work by testing the reliability of the blue emission lines directly against Hα, over the full range of galaxy types, SFRs, and nuclear properties.

Strictly speaking the fluxes of emission lines should be used to determine SFRs, but absolute line fluxes are difficult to measure in faint galaxies, due to effects of spatial undersampling, variable seeing, and atmospheric dispersion. Consequently, most analyses of distant galaxy spectra have been based on emission-line EWs, which can be determined much more reliably in faint sources. This section examines the relationships between the EWs of different features, in order to evaluate their general utility as SFR tracers. Approximate SFR calibrations based on the line fluxes are then derived for the most useful lines in § 5.

4.1. Hβ *and Other Balmer Lines*

From purely astrophysical considerations, the most reliable star formation tracers in the blue should be the higher order Balmer lines, since the fluxes of these lines-scale directly with the massive SFR and are nearly independent of the temperature and ionization level of the emitting gas. Figure 4 shows the relation between the EWs of Hβ and Hα + [N II]. Positive EWs denote net emission. The measurements include both the nebular emission and underlying stellar absorption components, so many galaxies exhibit negative EWs (net absorption). Solid symbols indicate spectra dominated by H II regions and diffuse interstellar emission, while open diamonds denote galaxies dominated by active nuclei. A few points with EW(Hα + N II) > 160 Å are off the scale of Figure 4, but those data follow the same general trends as shown.

A strong, roughly linear correlation between Hβ and Hα + [N II] EWs is apparent in Figure 4, especially among the galaxies dominated by star-forming H II regions. The solid line shows the relation expected for a simple model with f(Hα + N II)/f(Hβ) = 6, a flat continuum (f_λ) between Hβ and Hα, and a mean stellar absorption EW of 5 Å. Note that the

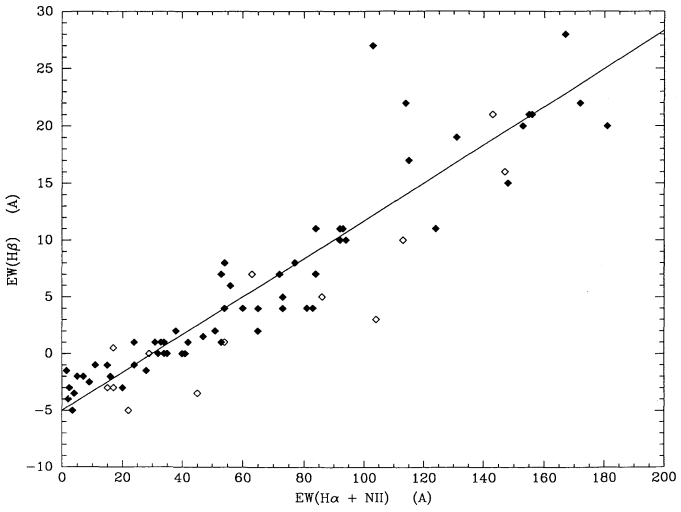

FIG. 4.—Relation between the equivalent widths of the Hβ and Hα + [N II] emission-line equivalent widths. Solid points are galaxies dominated by disk emission, and open symbols denote galaxies dominated by nonthermal nuclear emission. The line is a simple model with a constant stellar absorption equivalent width at Hβ, and a constant value for the Balmer decrement, as discussed in the text.

slope of this line is substantially different from the decrement $H\alpha/H\beta \simeq 3$ which is expected for H II regions with $T_e \sim$ 5000–10,000 K, even when allowance is made for the [N II] emission. The difference can be attributed to reddening. For an average [N II]/H$\alpha \simeq 0.5$ (§ 5.3), Figure 4 implies a mean absorption-corrected Balmer decrement $H\alpha/H\beta \simeq 4$, and a mean extinction $A_V \simeq 1$ mag. This is consistent with the mean optical extinction derived from other methods (e.g., Kennicutt 1983; Kennicutt et al. 1989). The scatter about the mean relation is roughly $\pm 30\%$, which presumably reflects variations in reddening, [N II]/Hα, and nuclear versus disk emission within the sample.

The correlation in Figure 4 confirms that the Hβ line can serve as a reliable star formation tracer in strong emission line galaxies, those with EW(Hα + N II) $\geq$ 60 Å, and EW(Hβ) $\geq$ 5 Å. This range includes the bluest Magellanic irregulars and starburst galaxies. Unfortunately Hβ is much less useful in normal galaxies (types E–Sc), which are characterized by EW(Hα + N II) $\leq$ 50 Å (Kennicutt & Kent 1983; Romanishin 1990). There stellar absorption dominates over the nebular emission line, and the net Hβ EW ranges from -5 Å (absorption) to $+3$ Å. For such galaxies, Hβ is only useful if its equivalent width is measured with very high precision [σ(EW) $\leq$ 1 Å], and the intrinsic strength of the stellar absorption line is known to comparable accuracy. At high spectral resolution and signal-to-noise ratio, the emission-line cores can be particularly resolved from the broader absorption features, and such a correction might be possible. For most applications, however, especially those relevant to studies of faint galaxies, the emission and absorption components will be blended, and the line will provide at best only an order-of-magnitude estimate (or lower limit) to the SFR. The higher order Balmer lines (Hγ, etc.) are even less reliable, because the effects of absorption become progressively worse farther up the Balmer series.

4.2. [O III] λ5007

Figure 5 shows the relation between the EWs of the [O III] λ5007 and Hα + [N II] lines. The symbols are the same as in Figure 4, except that ticks below a few points denote upper limits in [O III]. Here the situation is even worse. There is a very loose correlation between [O III] and Hα + [N II] EWs in the strongest emission-line galaxies, but the dispersion in this relation renders the [O III] fluxes virtually useless as quantitative SFR indicators. Among galaxies with normal SFRs, roughly EW(Hα + N II) $\leq$ 40 Å, the [O III] lines are rarely detected at all (EW $\leq$ 1–2 Å).

The most likely explanation for the dispersion in [O III]/Hα is a large variation in mean nebular excitation in disks, possibly combined with variations in the level of nuclear activity. The spiral galaxies observed at high resolution show a large range in the integrated [O III]/Hβ ratio, which is consistent with the large dispersion in excitation seen in spectroscopic surveys of H II regions in nearby galaxies (e.g., Zaritsky, Elston, & Hill 1990). Clearly the [O III] line has considerable value as an excitation diagnostic in high-redshift systems, but not as a quantitative SFR tracer.

4.3. [O II] λ3727

The [O II] λ3727 doublet is the most useful star formation tracer in the blue. Figure 6 shows the relation between the [O II] and Hα + [N II] EWs. Among galaxies dominated by stellar photoionization (*solid points*) the data follow a mean relation EW(O II) = 0.4 EW(Hα + N II), with an rms dispersion of $\sim$50%. This dispersion may be somewhat larger for galaxies with very strong emission lines (Hα EW > 100 Å). In addition to being the best behaved emission line in the blue, [O II] is the strongest feature after Hα + [N II]. This confirms the studies by Dressler & Gunn (1982), Dressler et al. (1985), Peterson et al. (1986), Broadhurst et al. (1988), and Gallagher et al. (1989), which maintained that the [O II] line can serve as a substitute for Hα in distant galaxies. An approximate calibration of the line is derived in the next section.

The [O II] versus Hα correlation breaks down for galaxies with luminous active nuclei (AGNs). These galaxies fall into two classes, those with abnormally strong [O II] emission, independent of Balmer line strength, and those with strong Balmer, [N II], and [O III] emission but weak (or undetected) emission in [O II]. The former most often are Seyfert 2 or

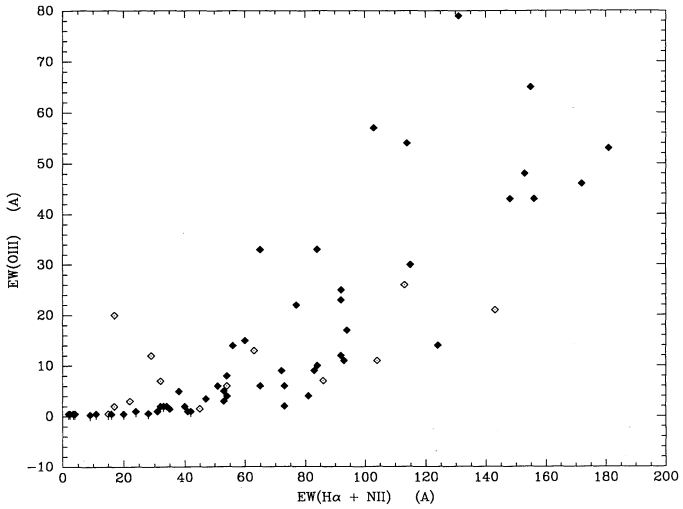

FIG. 5.—Relation between the equivalent widths of the [O III] λ5007 emission line and Hα + [N II]. Notation the same as in Fig. 4. Vertical lines denote upper limits in [O III].

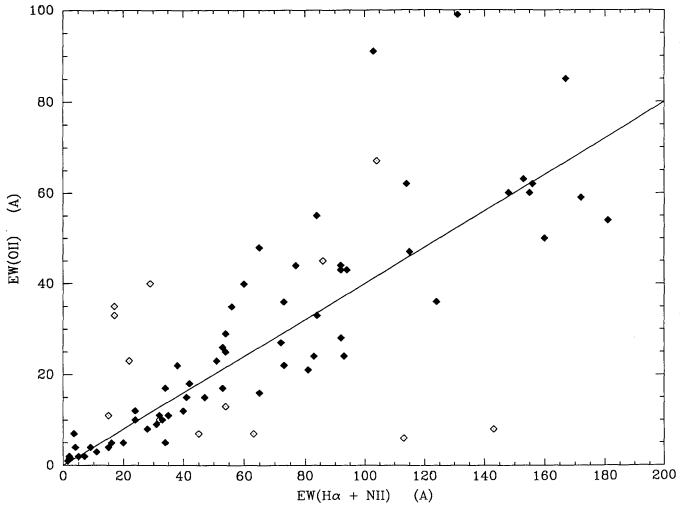

FIG. 6.—Relation between the equivalent widths of the [O II] λ3727 and Hα + [N II] emission lines. Notation the same as in Fig. 4. The line shows a simple model with EW(O II) = 0.4 EW (Hα + N II).

LINER nuclei, and the latter tend to be Seyfert 1 galaxies, though there are exceptions to this division.

4.4. *Emission Diagnostics*

When interpreting the emission-line spectra, it is important to be able to distinguish emission produced by star-forming regions from other sources such as active nuclei. Many distant AGNs have spectral signatures (blue continuum, strong [O II] emission) which closely mimic starbursting emission-line galaxies, and as a result such objects may be preferentially detected at high redshift (cf. Dressler & Gunn 1983). Here we use the spectra of nearby starbursting galaxies and AGNs to explore the most reliable means of separating the two classes of objects, when only an integrated spectrum is available.

The conventional means for distinguishing between gas ionized by stars and nonthermal processes are diagnostic line ratio diagrams (e.g., Baldwin et al. 1981). In our data, which extend to $\sim$7000 Å, it is quite easy to identify an AGN–dominated spectrum, either by the presence of strong [N II]/Hα relative to [O III]/Hβ, or by the detection of broad Balmer emission lines. The identification is much more difficult, however, when only the blue spectrum is available. The most powerful diagnostic features (e.g., [O I], [N II], [S II]) are no longer accessible, so the classification must be based on the [O II], [O III], and Hβ lines (plus whatever continuum information is available). The lack of an accurate reddening determination complicates the task further. Nevertheless these lines provide some interesting information, and it is useful to compare the diagnostic ratios in the integrated spectra to those in individual H II regions and nuclei.

Figure 7 shows the relation between the integrated [O III]/Hβ and [O II]/[O III] flux ratios for our sample, following the convention of Baldwin et al. (1981). In this case an approximate correction for the effects of stellar absorption on the [O III]/Hβ ratio has been applied, by assuming an Hβ absorption EW of 5 Å (see Fig. 4). Neither ratio has been corrected for reddening, however. As before, solid symbols denote galaxies which are dominated by star formation, while those dominated by nuclear emission are indicated by open symbols. In order to minimize the effect of spurious measurements, the sample was restricted to galaxies with EW(O II) $\geq$ 10 Å. The line in Figure 7 shows the mean reddening-corrected relation for stellar photoionized H II regions, taken from Baldwin et al. (1981).

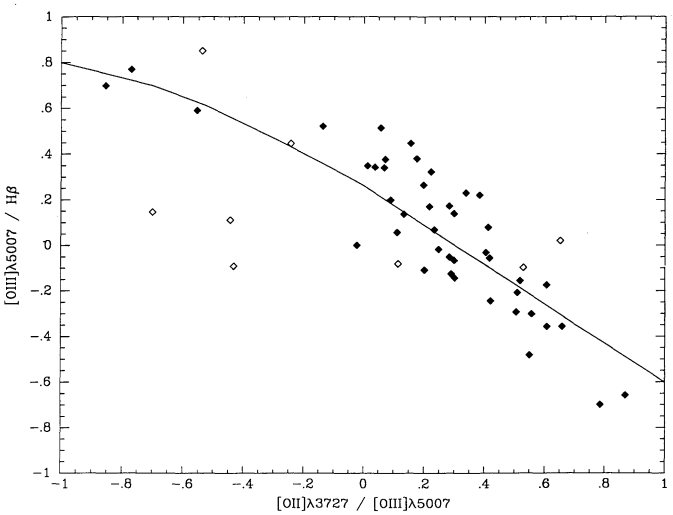

FIG. 7.—Diagnostic diagram for the integrated oxygen emission-line fluxes, following the convention of Baldwin, Phillips, & Terlevich (1981). Solid points denote galaxies dominated by disk emission, and open symbols indicate galaxies with emission dominated by a nonthermal nucleus. The line shows the mean relation for H II regions in the Baldwin et al. study. The [O III]/Hβ ratios have been corrected for stellar Balmer absorption. The data shown here have not been corrected for reddening, so most points lie farther to the right than indicated here.

The star-forming galaxies generally follow the relation expected for H II regions. This suggests that such integrated spectra could be used to crudely derive a characteristic excitation, and perhaps even the mean metal abundance of a galaxy, using an empirical abundance calibration such as the one proposed by Edmunds & Pagel (1984). Any such abundance estimates would require accurate measurements of the [O III], [O II], and Hβ fluxes, corrected for stellar absorption. The only possible deviation from the main H II region relation is a tendency for most of the high-excitation points ([O III]/H$\beta \geq$ 1) lie to the right of the H II region relation (high [O II]/[O III]). The formal significance of the trend in the raw data is marginal, but correcting the [O II]/[O III] ratios for reddening (not possible with the available data), would drive the points toward the right in this diagram, suggesting that the apparent excess in [O II]/[O III] is probably real. Inspection of the spectra shows that this excess is due to unusually high [O II]/Hβ ratios (rather than low [O III]/Hβ) when compared to bright H II regions. We tentatively attribute this excess to emission from diffuse interstellar gas, which typically exhibits much lower ionization and stronger [O II] emission than H II regions (e.g., Hunter 1984; Hunter & Gallagher 1990). Many of the galaxies in our sample with the strongest [O II] (e.g., NGC 4449, 4485) show extensive diffuse nebulosity in direct images.

A few of the AGNs lie well off the mean relation for star-forming galaxies, especially the three Seyfert 1 galaxies with low [O II]/[O III]. Most of the AGNs, however, including most of the Seyfert 2 galaxies in our sample, are sufficiently close to the main relation that they cannot be identified on the bases of these line ratios alone. This is not surprising; analyses of nearby galaxies by Baldwin et al. (1981) and others demonstrate that additional features such as [N II] λ6583 or [O I] λ6300 are often required for an unambiguous separation.

A more effective means of discriminating distant AGNs from star-forming galaxies is to correlate [O II] strength with continuum color, as proposed originally by Dressler & Gunn (1982). Figure 8 shows the logarithm of the [O II] EW plotted against the 41–50 color index, as defined in equation (1). Note that this definition differs from that used by Dressler et al. (1985). Solid and open diamonds denote normal and AGN–dominated galaxies from this survey, while solid circles are data for 32 nearby field and cluster galaxies (crosses denote upper limits) from Dressler et al. (1985). The new data allow us to extend the relation for star-forming galaxies by nearly an order of magnitude higher in EW(O II), and this is critical for separating starbursts from AGNs, since many of the latter show EW(O II) $\geq$ 30 Å.

Overall there is a well-defined relation between [O II] strength and color (cf. Dressler et al. 1985), which parallels the Balmer EW versus color relation for galaxies (Cohen 1976; Huchra 1977; Kennicutt & Kent 1983). There is also a clear separation between the normal galaxies and most of the AGNs. Seyfert 2 galaxies tend to fall to the right of the main relation, which is expected because the Seyfert nuclei tend to occur in early to intermediate-type spirals, which have much redder colors than star-forming emission line galaxies. Many

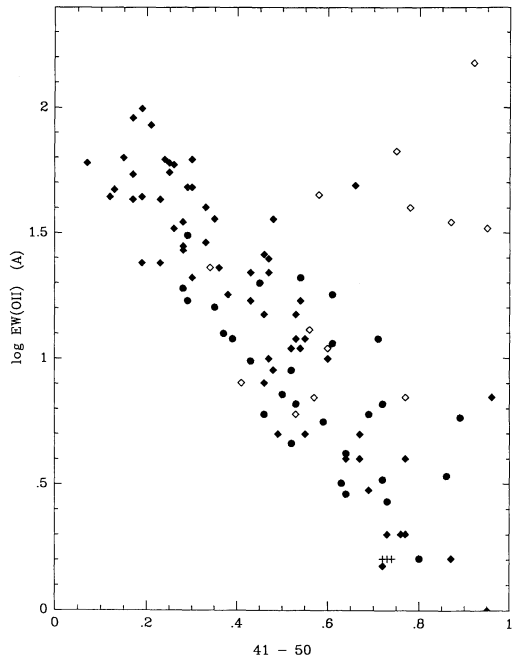

FIG. 8.—Relation between the logarithm of the [O II] λ3727 equivalent width and continuum color, as defined in the text. Solid diamonds and points are galaxies dominated by disk emission, from this survey and from Dressler et al. (1985), respectively. Plus marks are upper limits from Dressler et al. Open symbols are galaxies from this survey with emission dominated by a nonthermal nucleus.

of the Seyfert 1 galaxies lie below the main relation, but the separation is less clean, and some do not deviate from the main relation at all. Seyfert 1 galaxies can usually be identified by other criteria, however, such as broad emission lines or by the emission line ratios (Fig. 7). The [O II] versus color relation offers an especially powerful means of discriminating between star-forming emission-line galaxies and Seyfert 2 nuclei, which are often difficult to identify on the basis of the emission spectrum alone.

The utility of the EW versus color relation for identifying distant AGNs is not a new result; it merely confirms the conclusions reached earlier by Dressler & Gunn (1982) and Dressler et al. (1985). It is important to point out, however, that the dividing line between AGNs and starburst galaxies in Figure 8 is quite different from that which was extrapolated in the previous work. This will alter the identifications of some of the AGNs in those surveys.

5. DISCUSSION

The strong correlation between [O II] and Hα + [N II] EWs (Fig. 6) suggests that the [O II] luminosity ought to be usable as a quantitative indicator of the SFR in a distant galaxy, in much the same way that Hα is used in nearby galaxies. Since the [O II] feature can be readily observed from the ground to redshifts of at least unity, they provide a powerful means of studying the systematics of galactic star formation to cosmological redshifts and lookback times, confirming the previous work by Dressler & Gunn (1982), Peterson et al. (1986), and Gallagher et al. (1989).

In this section we discuss several aspects of the [O II] emission in nearby galaxies which are most relevant to their application in surveys of faint objects. We first discuss the statistical properties of the [O II] EWs in the local sample, and then derive approximate calibrations between the [O II] fluxes and the integrated SFR. We conclude by discussing the optimal strategy for estimating SFRs from the UV and optical spectra of distant galaxies.

5.1. *Distribution of* [O II] *Equivalent Widths*

Broadhurst et al. (1988) and Colless et al. (1990) have used the distribution function of rest-frame [O II] EWs to compare the star formation properties of galaxies at $z \simeq 0.2$–0.3 to $\bar{z} \simeq 0.05$. The apparent excess of strong [O II] galaxies in the high-redshift samples is one of the strongest pieces of empirical evidence for subtantial evolution in the field galaxy population with cosmological lookback time. Such comparisons require a reference sample of nearby galaxies which is free of selection biases in either the sample itself or in the spectrophotometry. In the studies cited above, the reference sample was the $B = 17$ limited "DARS" survey of 340 field galaxies by Peterson et al. (1986). The DARS observations were made with narrow slits which undersample the galaxies, and some concern has been expressed by Broadhurst et al. (1988) and Colless et al. (1990) as to whether this effect could produce part of the apparent evolution in the [O II] EW distributions. Although the sample of galaxies observed here is much smaller than the DARS, its selection properties are well understood, and it can be used to provide an independent measurement of the local [O II] EW distribution, for comparison with the DARS results.

The present survey is by no means complete, but the subsample of normal E–Irr galaxies was deliberately selected with approximately the same distribution of morphological types as the Revised Shapley-Ames Catalog (Sandage & Tammann 1981, hereafter RSA). This sample consists of 37 normal elliptical, S0, spiral, and Magellanic irregular galaxies (including nine E/S0 galaxies which are not listed in Tables 1–2), and excludes I0 galaxies and peculiar objects which had been selected based on blue colors, nuclear activity, etc. The fraction of galaxies in the bins E–S0, Sa–Sab, Sb–Sbs, Sc–Sd, and Sm–Im (see Table 4) matches the RSA to within a few percent. Hence it should provide a reasonable approximation, within sampling errors, of a local magnitude-limited EW distribution.

A second estimate of the local [O II] distribution can be derived if one takes advantage of the strong correlation between [O II] and Hα + [N II] EWs (Fig. 6). Hα + [N II] data are available for roughly 140 nearby galaxies from Kennicutt & Kent (1983), and a local distribution of Hα + [N II] EW was derived by compiling an EW histogram for each Hubble type separately, and averaging these with weights proportional to the distribution of morphological types in the RSA. This was then rescaled to [O II], using a mean EW(O II)/EW(Hα + N II) ratio of 0.4 (§ 4.3). This rescaling of the Hα distribution clearly is no substitute for the actual [O II] mea-

TABLE 4

MEAN [O II] EQUIVALENT WIDTHS

TYPE	⟨EW⟩ (Number) Normal Galaxies	All Galaxies	DARS
E, S0	1.3 (9)	23.9 (14)	2.7 (55)
Sa, Sab	2.3 (7)	5.9 (11)	8.5 (24)
Sb, Sbc	6.7 (9)	16.1 (15)	10.8 (38)
Sc, Scd, Sd	17.4 (10)	29.7 (22)	9.4 (36)
Sm, Im	48.3 (2)	54.1 (21)	29.6 (4)

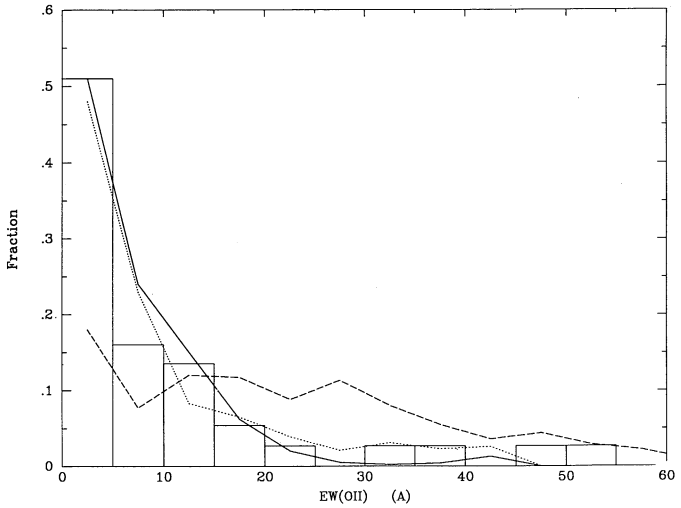

FIG. 9.—Frequency distributions of [O II] λ3727 equivalent width in the spectra of galaxies. *Histogram:* 37 normal galaxies in this sample with measured [O II] EWs. *Solid line:* 149 galaxies with measured Hα + [N II] EWs, scaled to [O II] as described in text. *Dotted line:* DARS sample of nearby galaxies by Peterson et al. (1986). *Dashed line:* Durham faint galaxy samples of Broadhurst et al. (1988) and Colless et al. (1990). A few percent of the galaxies in the Durham sample lie off the right end of the plot.

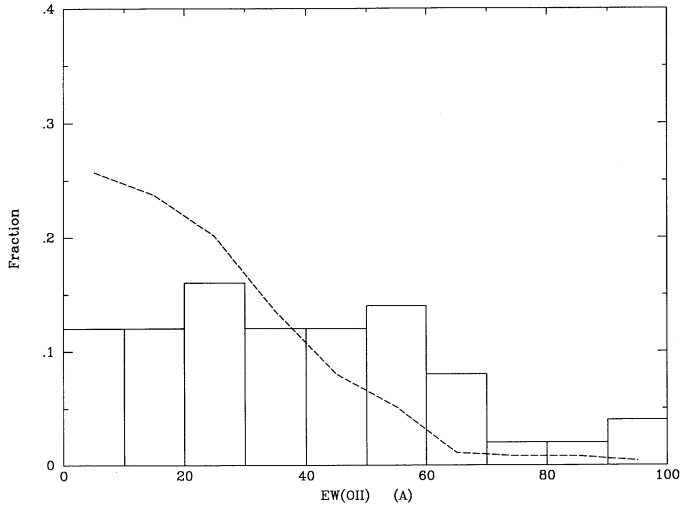

FIG. 10.—Frequency distributions of [O II] λ3727 equivalent widths. *Histogram:* nearby Markarian galaxies from this survey and Gallagher et al. (1989). *Dashed line:* Durham faint galaxy samples, as in Fig. 9.

surements, but it provides a secondary check based on a much larger sample.

Figure 9 compares the two EW distributions discussed above with the DARS distribution. Also shown is the combined distribution for the Durham/AAT faint galaxy samples (Broadhurst et al. 1988; Colless et al. 1990). The three distributions derived from nearby galaxy samples are very similar, and the slight differences are all within the statistical errors of the current survey. The largest single difference is the excess of galaxies in this survey with EW ≥ 40 Å, and this can be attributed directly to an overrepresentation of Magellanic irregulars in the sample, 2/37 or 5% here, versus only 2% in the RSA.

On the other hand, the distribution for the faint, distant galaxy sample (Fig. 9, *dashed line*) shows the well-known excess of galaxies with high [O II] EWs. The subtle differences between the nearby galaxy samples, if significant at all, are small in comparison to the changes with redshift. We conclude that the [O II] emission line properties of the DARS sample are representative of the nearby galaxy distribution, and that the excess of [O II] strong galaxies observed in the faint surveys cannot be attributed to any selection effects in the nearby comparison samples.

Although the strong emission-line galaxies observed in the more distant samples lie in the extreme high-EW tail of the local [O II] distribution, local analogs are easily found, as discussed by Gallagher et al. (1989). For example, Figure 10 shows the [O II] EW distribution for 49 Markarian galaxies in the current survey plus Gallagher et al. (1989), compared to the respective distributions for the intermediate-redshift samples of Broadhurst et al. (1988) and Colless et al. (1990). The Markarian samples includes galaxies with upper limits to the [O II] EWs (all below 10 Å). Markarian galaxies were identified on the basis of strong UV continuum on objective prism plates, so they might be expected to represent the same kinds of emission-line galaxies that are found at high redshift. Figure 10 confirms that the [O II] properties of the two samples are indeed similar. This comparison is merely illustrative; the Markarian subsample is far too incomplete and inhomogeneous to be representative of even a local blue galaxy population, and a proper comparison would need to take into account the respective luminosity functions and space densities of the respective populations. The comparison does offer an impressive illustration, however, of how radically the [O II] distributions can change if a UV color-weighted selection criterion is used to define the galaxy sample.

5.2. [O II] *Emission versus Morphological Type*

Figure 11 shows the dependence of [O II] EW on galaxy type, for normal (*solid points*) and peculiar galaxies (*open symbols*). In this case we have defined as "peculiar" not only galaxies with AGNs, but also those which were selected for the survey on the basis of unusually blue colors, evidence of strong interactions, etc. The mean EWs for each type are given in Table 4, along with the same values from the much larger DARS survey (Peterson et al. 1986). The normal galaxies in our sample show a smooth increase in mean EW with type, which parallels the relation for Hα (e.g., Kennicutt & Kent 1983). This

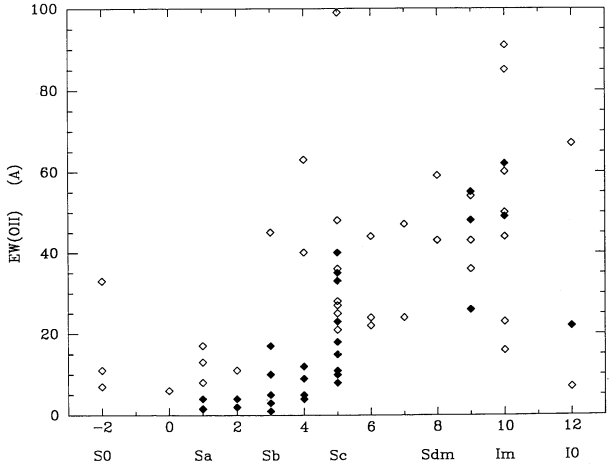

FIG. 11.—Distribution of [O II] λ3727 equivalent widths vs. galaxy type. Numbers are de Vaucouleurs types.

is somewhat different from the behavior of the DARS sample, which shows a significant change in EW from the S0 to spiral to irregular classes, but no gradient in EW within the spiral sequence. The differences cannot be attributed entirely to statistical uncertainties, and we suspect that they arise from classification errors in the DARS, and the fact that peculiar galaxies are included in the DARS averages, but not in ours. When applying the results of Figure 11 or Table 2 to distant galaxies, one should also bear in mind that the relationship between morphological type and spectral type may itself evolve with lookback time.

5.3. [O II] *Luminosities and Total Star Formation Rates*

Kennicutt (1983) calibrated the relationship between the integrated Hα luminosity and total SFR in disk galaxies, and the spectrophotometry presented here can be used to derive a corresponding relation between [O II] flux and SFR.

Figure 12 shows the distribution of the [O II]/(Hα + N II) flux ratio for the sample. The total Hα + [N II] flux has been used, rather than Hα alone, because the lines are blended in part of the sample, and most photometric measurements of Hα in nearby galaxies include the [N II] lines. The median value for [O II]/(Hα + N II) is 0.31 for the entire sample, or 0.30 is AGNs and peculiar galaxies are excluded. The corresponding median EW ratio for these lines is 0.4 (Fig. 6); the difference reflects the mean continuum slope between 3727 and 6570 Å.

In order to convert the Hα SFR scale to [O II] we also need a value for the average [N II]/Hα ratio. The median value measured for our sample is 0.53 (excluding Seyfert galaxies). This is considerably higher than the value of 0.33 which was derived by Kennicutt & Kent (1983), using published spectra of extragalactic H II regions. Several factors contribute to this difference. Stellar absorption of Hα, not included by Kennicutt & Kent, is important in early-type galaxies. Nuclear emission, which was not explicitly included in the Kennicutt & Kent analysis, probably raises the mean integrated [N II]/Hα ratio. Diffuse interstellar gas, which has a higher characteristic [N II]/Hα strength than in H II regions (e.g., Hunter & Gallagher 1990), probably contributes to the difference as well. Finally, the mean [N II]/Hα value derived here may be slightly biased toward high values, because galaxies with blended lines are not included, and this will preferentially exclude objects with low [N II]/Hα from the sample. If we adopt a tentative [N II]/Hα value of 0.5, the calibration between SFR and Hα luminosity from Kennicutt (1983),

$$R(M_\odot\ \mathrm{yr}^{-1}) = 8.9 \times 10^{-42} L(\mathrm{H}\alpha) E(H\alpha)\ ,$$

now can be transformed to [O II] luminosity:

$$R(M_\odot\ \mathrm{yr}^{-1}) = 2.0 \times 10^{-41} L(\mathrm{O\ II}) E(\mathrm{H}\alpha)\ .$$

In these equations L is the observed emission line luminosity in units of ergs s^{-1}, and E is the extinction correction factor at Hα; since the mean [O II]/(Hα + N II) ratios are observed values, uncorrected for reddening, no additional correction for extinction at [O II] is required. For nearby spirals $\bar{E} \simeq 1.0$ mag (Kennicutt 1983; this paper), and applying this factor yields an extinction-corrected calibration

$$R(M_\odot\ \mathrm{yr}^{-1}) \simeq 5 \times 10^{-41} L(\mathrm{O\ II})\ .$$

The corresponding SFRs for massive stars only ($M \geq 10\ M_\odot$) are a factor of 6.3 lower, if the IMF in Kennicutt (1983) is used.

Gallagher et al. (1989) also derived SFR calibrations for L(O II), based on [O II] and Hβ spectrophotometry of a nearby blue irregular galaxies. Their calibration factors in equations (3) and (4) are lower than ours (lower SFR for same [O II] luminosity) by factors of 3 and 5, respectively. Part of the difference reflects the lower extinction and reddening in irregulars as compared to spirals, and a small (25%) difference in the IMFs and stellar models used by Kennicutt (1983) and Hunter & Gallagher (1986). In that respect the difference in the calibrations can be taken to be a conservative estimate of the uncertainties in deriving the SFRs. Gallagher et al. also were forced to extrapolate to Hα using an assumed value for the Balmer decrement, and the theoretical Hα/Hβ ratio they used (2.86) is lower than the mean absorption-corrected value of ~4 measured in our sample. Equation (4) is probably a reasonably accurate *mean* relation for distant spiral galaxies, but for very blue, metal-poor galaxies, the SFRs could be as much as a factor of three lower than given by equation (4).

One drawback of equations (3) and (4) for applications to distant galaxies is that they require a photometric measurement of the [O II] flux, whereas most surveys of faint galaxies are optimized for redshift determinations, and only the [O II] EW is available. In such cases an approximate SFR can be derived if the EW and integrated broadband magnitude are known. [O II] luminosities were derived for 16 galaxies in this survey, using the [O II]/(Hα + N II) ratios in Tables 1–2, and Hα + [N II] luminosities from Kennicutt & Kent (1983). The mean relation between [O II] luminosity, EW(O II), and B luminosity was then fitted to the data:

$$L(\mathrm{O\ II}) \sim 1.4 \pm 0.3 \times 10^{29} \frac{L_B}{L_B(\odot)}\ \mathrm{EW(O\ II)\ ergs\ s^{-1}}\ .$$

Combining equations (3) and (5) yields

$$R(M_\odot\ \mathrm{yr}^{-1}) \sim 2.7 \times 10^{-12} \frac{L_B}{L_B(\odot)}\ \mathrm{EW(O\ II)} E(\mathrm{H}\alpha)\ .$$

In both equations above the B luminosity is expressed in units of the B luminosity of the Sun ($M_B = 5.48$), and the inclination-corrected absolute magnitudes from Sandage & Tammann (1981) were used. If we adopt the same extinction correction as

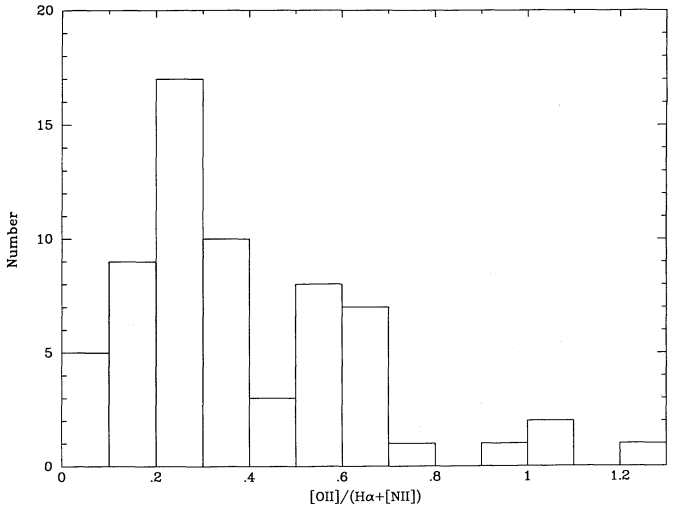

FIG. 12.—Distribution of the ratio of flux in the [O II] λ3727 and Hα + [N II] emission lines for this sample. Values are not corrected for reddening or stellar absorption at Hα.

used earlier in equation (4), the coefficient in the above equation becomes 7×10^{-12}. The reader should beware that the error in these SFRs is considerably larger than those derived using equations (3) and (4), because the relations are adopting a mean slope for the continuum between the mean wavelength of the B bandpass ($\sim$4400 Å) and 3727 Å. Inspection of Figures 2 and 3 reveals a dispersion of more than a factor of 2 in this ratio, and this will introduce a proportional error into the SFRs, in addition to the other errors inherent in the [O II] flux itself as a star formation tracer. Hence the "SFRs" derived from equation (7) should be regarded as rough estimates, rather than quantitative measures of the SFR. However, the equation may be useful for characterizing the approximate level of star formation in a sample of distant objects.

5.4. *Strategies for Measuring Star Formation Rates in Distant Galaxies*

While the calibrations provided above provide a convenient means of estimating the total SFR in any distant galaxy with a measured [O II] flux or EW, the uncertainties in the resulting SFRs are much larger than those derived from Hα. Here we consider those errors in quantitative terms, and compare the accuracy of the [O II]–based SFRs with other methods.

As is the case for SFRs derived from the Hα line, the dominant errors are not from observational uncertainties but rather from systematic effects. The largest single source of dispersion for [O II] is the large variation in excitation, as illustrated in Figure 12. Unlike the Balmer line fluxes, which scale directly with the number of ionizing stars, the accuracy of [O II] is limited by the variation in the [O II]/Hα (or [O II]/Hβ) ratio. The 1 σ range in the ratio of Hα + [N II] to [O II] fluxes is 1.7–5.6 for our sample, corresponding to an rms dispersion of $\pm$80% in any single SFR, on top of any systematic error in the Hα-based SFR calibration itself. Over the entire sample the Hα + [N II] to [O II] ratio varies from less than unity to over 20. This dispersion in "excitation" is due to a combination of true variations in nebular excitation (see Fig. 7) as well as variations in reddening. The mean [O II]/Hα + [N II] ratio also shows some systematic variation, from 0.24 for galaxies with EW(Hα + [N II]) < 50 Å to 0.36 for those with EW $\geq$ 50 Å. This can introduce systematic errors in SFRs at the 50% level if disparate samples of galaxies are compared.

SFRs derived from the [O II] line will also be subject to the same systematic errors that affect the Hα-based SFR scale. These have been discussed in detail by Kennicutt (1983, 1990). The dominant systematic errors are due to uncertainties in the corrections for extinction, variations in the initial mass function (IMF), and possibly the escape of ionizing radiation from the galaxies. Kennicutt (1983) estimated that the combined uncertainty from these effects limited the accuracy of the SFR for an individual galaxy to typically $\pm$30%–50%. When one adds these uncertainties to the additional dispersion in excitation for [O II], it is clear that an SFR derived for an individual galaxy based on its [O II] flux alone will only be accurate to within a factor of a few.

The limited precision of the [O II] SFR calibration means that other methods for estimating the total SFR, such as the UV–blue colors and magnitudes, become competitive alternatives. For example, SFRs estimated from the UBV colors and blue luminosities of galaxies (e.g., Searle, Sargent, & Bagnuolo 1973; Larson & Tinsley 1978) have an accuracy which is a strong function of color and reddening, ranging from factors of 2–3 in blue galaxies to factors of several on red spirals, or in heavy reddened objects (see Figs. 3 and 7 in Kennicutt 1986). If precise measurements of the near-ultraviolet continuum flux are fitted to synthetic energy distributions (e.g., Bruzual 1983), somewhat higher accuracy might be expected.

Given these results, what is the best strategy for estimating the global SFR in a distant galaxy for which only an integrated spectrum is available? The answer depends critically on the nature of the available data. For galaxies in which the continuum energy distributions have been accurately determined, the continuum colors and fluxes are likely to yield SFRs with comparable or better accuracy than the [O II] line. In those cases, the best recommendation is probably to rely on the continuum data but apply the [O II] flux as a check. In many data sets, however, especially those obtained using multi-object spectrographs, the signal-to-noise ratio and calibration of the continuum colors are poor, and in those cases the [O II] flux (or the [O II] EW combined with an integrated magnitude) probably offer the most reliable means of characterizing the star formation properties of the galaxy.

This survey benefited from the help of several individuals. The 2.3 m telescope operators at Steward Observatory, Dennis Means, Gary Rosenbaum, and Vic Hansen, offered capable and patient assistance with the unorthodox drift scanning observations, and University of Minnesota graduate students Joni Johnson and Dimitri Klebe assisted with the observations at KPNO. Charles Congdon worked on the early stages of the data analysis, and Jeannette Barnes assisted with the IRS data reduction. The referee, G. Bothun, provided very constructive criticisms and suggestions which improved the paper. This work was supported by NSF grants AST-8613257 to the University of Minnesota, and AST-8996123 and AST-9090150 to the University of Arizona.

REFERENCES

Baldwin, J. A., Phillips, M. M., & Terlevich, R. 1981, PASP, 93, 5
Barnes, J. V., Massey, P., & Carder, E. 1986, IRS Instrument Manual, Kitt Peak National Observatory
Bothun, G., & Dressler, A. 1986, ApJ, 301, 57
Broadhurst, T. J., Ellis, R. S., & Shanks, T. 1988, MNRAS, 235, 827
Bruzual, A. G. 1983, ApJ, 273, 105
Cohen, J. G. 1976, ApJ, 203, 587
Colless, M., Ellis, R. S., Taylor, K., & Hook, R. N. 1990, MNRAS, 244, 408
Couch, W. J., & Sharples, R. M. 1987, MNRAS, 229, 423
de Vaucouleurs, G., de Vaucouleurs, A., & Corwin, H. G. 1976, Second Reference Catalog of Bright Galaxies (Austin: Univ. of Texas Press)
Dressler, A., & Gunn, J. E. 1982, ApJ, 263, 533
———. 1983, ApJ, 270, 7
Dressler, A., Gunn, J. E., & Schneider, D. P. 1985, ApJ, 294, 70
Edmunds, M. G., & Pagel, B. E. J. 1984, MNRAS, 211, 507
Elston, R., Bechtold, J., Lowenthal, J., & Rieke, M. 1991, ApJ, 373, L39
Gallagher, J. S., Bushouse, H., & Hunter, D. A. 1989, AJ, 97, 700
Gallagher, J. S., Hunter, D. A., & Tutukov, A. V. 1984, ApJ, 284, 544
Huchra, J. P. 1977, ApJS, 35, 171
Hunter, D. A. 1984, ApJ, 276, L35
Hunter, D. A., & Gallagher, J. S. 1986, PASP, 98, 5
———. 1990, ApJ, 362, 480
Kennicutt, R. C. 1983, ApJ, 272, 54
———. 1986, in Stellar Populations, ed. C. Norman, A. Renzini, & M. Tosi (Cambridge: Cambridge Univ. Press), 125
———. 1990, in The Interstellar Medium in Galaxies, ed. H. A. Thronson & J. M. Shull (Dordrecht: Kluwer), 405
———. 1992, ApJS, 79, 255 (Paper II)
Kennicutt, R. C., Bothun, G. D., & Schommer, R. A. 1984, AJ, 89, 1279
Kennicutt, R. C., Keel, W. C., & Blaha, C. A. 1989, AJ, 97, 1022
Kennicutt, R. C., Keel, W. C., van der Hulst, J. M., Hummel, E., & Roettiger, K. 1987, AJ, 93, 1011
Kennicutt, R. C., & Kent, S. M. 1983, AJ, 88, 1094
Larson, R. B., & Tinsley, B. M. 1978, ApJ, 219, 46
Lavery, R. J., & Henry, J. P. 1988, ApJ, 330, 596
Morgan, W. W. 1958, PASP, 70, 364

Morgan, W. W., & Mayall, N. U. 1957, PASP, 69, 291
Morgan, W. W., & Osterbrock, D. E. 1969, AJ, 74, 515
Peterson, B. A., Ellis, R. S., Bean, A. J., Efstathiou, G., Shanks, T., Fong, R., & Zou, Z.-L. 1986, MNRAS, 221, 233
Pickles, A. J., & Visvanathan, N. 1985, ApJ, 294, 134
Romanishin, W. 1990, AJ, 100, 373
Sandage, A., & Tammann, G. A. 1981, A Revised Shapley-Ames Catalog of Bright Galaxies (Washington, DC: Carnegie Institution of Washington) (RSA)
Searle, L., Sargent, W. L. W., & Bagnuolo, W. G. 1973, ApJ, 179, 427
Silva, D. R. 1991, Ph.D. thesis, Univ. Michigan
Weedman, D. W. 1977, ARA&A, 15, 69
Wells, D. G. 1972, Ph.D. thesis, Univ. Texas
Zaritsky, D., Elston, R., & Hill, J. M. 1990, AJ, 99, 1108